Diffraction from Small Volumes

17

CHAPTER PREVIEW

A very important concept in TEM is that we only diffract from small volumes. By definition, no specimens are infinite in all directions and all defects are small. Of course, the beam is also never infinitely wide! This chapter therefore discusses how the size of what we are examining influences the appearance of the DP. Although we will discuss many different aspects of diffraction, there are three important ideas which underlie all this discussion:

- We are diffracting from small volumes.
- We are diffracting from crystals.
- We need to index the DPs we see and relate the patterns to the image.

The fact that it is possible to obtain diffraction from several planes in a zone at the same time is due to the effect of the specimen shape on the diffracted-intensity distribution. The diffraction spot is only a mathematical point if the specimen is perfect and infinite in all directions. For example, a TEM specimen is effectively infinite (~3 mm) relative to the unit-cell dimensions in the plane of the specimen, but very thin (< 0.5 μm) parallel to the electron beam. This means that the diffracted intensity can be represented in the reciprocal lattice as a rod stretched parallel to the electron beam in reciprocal space, rather than as a point, and the rod does have a width. Therefore, over a range of angles, the Ewald sphere will still intercept the rod and diffracted intensity will still be generated. This is equivalent to saying that the Laue condition is relaxed in one dimension in the TEM

D. B. Williams et al., *Transmission Electron Microscopy*

owing to the specimen shape. For this reason, accurate structural analysis of unknown specimens is very difficult in conventional TEM diffraction, and X-rays are usually the most accurate method for structure determination if your specimen is large. However, we will reconsider this statement in Chapter 21.

Diffraction from Small Volumes

17

17.1. INTRODUCTION

In Chapter 12, we stated that each point in the reciprocal lattice can actually be associated with a rod. This construction allowed us to discuss the geometry of DPs, taking account of the experimental fact that we see spots in the DP even when **s** is not exactly zero. In fact, without this construction, there is no reason to discuss **s**. Now we are going to show quantitatively why we have rods. As we suggested earlier, the reason is that we have a thin specimen: a small thickness in real space gives a large length in reciprocal space. This concept is valid in all directions, not just parallel to the electron beam. Hence, we call this the "shape effect." The intensity in the diffracted beam is generally strongest when $\mathbf{K} = \mathbf{g}$, but we still have intensity when **K** is not exactly equal to **g**, or when

$$\mathbf{K} = \mathbf{g} + \mathbf{s} \qquad [17.1]$$

Then we can write, from equation 13.48

$$|\phi_{\mathbf{g}}|^2 = \left(\frac{\pi t}{\xi_{\mathbf{g}}}\right)^2 \frac{\sin^2(\pi t s_{\text{eff}})}{(\pi t s_{\text{eff}})^2} \qquad [17.2]$$

We model the specimen as a thin rectangular slab as shown in Figure 17.1. To keep the math simple, we will assume that we have a rectangular unit cell with sides a, b, c and that there are N_x cells in the x direction, N_y in the y direction, and N_z in the z direction. All that we have to do to determine the total diffracted amplitude is to add the amplitudes from each cell, allowing for the phase factor, because the cells are displaced from one another. Each cell has the same structure factor F.

We can do the addition of amplitudes in two ways. The first way is to do the summation. In the second, we will show how the same result follows if you start with the integral expression for $\phi_{\mathbf{g}}$. These expressions lead to the important idea of a relrod and subsidiary maxima; in DPs we can see the effects of the relrods, but we usually don't see the subsidiary maxima.

What we are going to do is derive equations for the shape of the relrods which were used in Chapter 13 to explain why we see spots in the DP even when $\mathbf{s} \neq 0$. This whole approach gives us a pictorial aid to understanding diffraction from small volumes. After developing the theory for the simple case, we will go on to discuss the complications introduced because we look at real materials, and specimens of real materials are usually not flat platelets.

17.1.A. The Summation Approach

This approach starts with expressing the total amplitude, A, of the diffracted beam as the sum of contributions from all the individual cells in a parallel-sided specimen

$$A = F \sum_{n_x} e^{i2\pi n_x \mathbf{K}\cdot\mathbf{a}} \sum_{n_y} e^{i2\pi n_y \mathbf{K}\cdot\mathbf{b}} \sum_{n_z} e^{i2\pi n_z \mathbf{K}\cdot\mathbf{c}} \qquad [17.3]$$

Here n_x, n_y, and n_z have their usual meanings and all are integers. As shown in Figure 17.1, we will let n_x vary from 0 to $N_x - 1$, and similarly with n_y and n_z. The location of each unit cell is then defined by the vector $\mathbf{r}_n$

$$\mathbf{r}_n = n_x\mathbf{a} + n_y\mathbf{b} + n_z\mathbf{c} \qquad [17.4]$$

To simplify the first summation we set X equal to $e^{i2\pi\mathbf{K}\cdot\mathbf{a}}$, then each separate summation term is a geometric series, so we can sum the n_x terms as

$$S = \sum_{n_x=0}^{n_x=N-1} X^n = X^0 + X^1 + \cdots X^{N-1} = \frac{1 - X^N}{1 - X} \qquad [17.5]$$

(Remember, if you multiply S by X you get $S + X^N - X^0$ and $X^0 = 1$.)

Summing from $n_x = 0$ to $n_x = N_x - 1$ we obtain

$$\sum_{n_x=0}^{n_x=N-1} e^{i2\pi n_x \mathbf{K}\cdot\mathbf{a}} = \frac{1 - e^{i2\pi n_x \mathbf{K}\cdot\mathbf{a}}}{1 - e^{i2\pi \mathbf{K}\cdot\mathbf{a}}} \qquad [17.6]$$

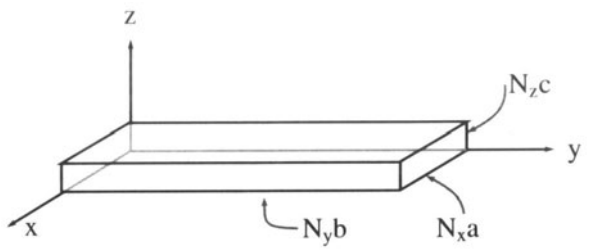

Figure 17.1. An idealized thin-foil specimen modeled as a rectangular slab made up of rectangular unit cells of sides a, b, c. There are N_x cells in the x direction, N_y in the y direction, and N_z in the z direction.

Since we are interested in the intensities, we multiply this sum by its complex conjugate. To do this we use some simple trigonometric relationships

$$\begin{aligned}&\left(1-e^{-i\alpha}\right)\left(1-e^{i\alpha}\right)\\&=\left(1-\cos\alpha+i\sin\alpha\right)\left(1-\cos\alpha-i\sin\alpha\right)\\&=\left(1-2\cos\alpha+\cos^2\alpha\right)+\sin^2\alpha\\&=2\left(1-\cos\alpha\right)=4\sin^2\frac{\alpha}{2}\end{aligned} \qquad [17.7]$$

The intensity is then related to

$$\left|\sum_{n_x=0}^{n_x=N-1} e^{i2\pi n_x \mathbf{K}\cdot\mathbf{a}}\right|^2 = \frac{1-\cos\left(2\pi N_x \mathbf{K}\cdot\mathbf{a}\right)}{1-\cos\left(2\pi\,\mathbf{K}\cdot\mathbf{a}\right)} \qquad [17.8]$$

Then we can write

$$\begin{aligned}&I=|A|^2\\&=|F|^2\left(\frac{\sin^2(\pi N_x\mathbf{K}\cdot\mathbf{a})}{\sin^2(\pi\,\mathbf{K}\cdot\mathbf{a})}\right)\left(\frac{\sin^2(\pi N_y\mathbf{K}\cdot\mathbf{b})}{\sin^2(\pi\,\mathbf{K}\cdot\mathbf{b})}\right)\left(\frac{\sin^2(\pi N_z\mathbf{K}\cdot\mathbf{c})}{\sin^2(\pi\,\mathbf{K}\cdot\mathbf{c})}\right)\end{aligned} \qquad [17.9]$$

If the dot product $\mathbf{K}\cdot\mathbf{a}$ is an integer, then the first of these terms is unity. This is, of course, the Bragg condition and the intensity is then a maximum. There are also subsidiary maxima or minima when

$$\pi N_x\mathbf{K}\cdot\mathbf{a}=\frac{\pi}{2}C \qquad [17.10]$$

where C = an integer. Reordering this equation, we have

$$\mathbf{K}\cdot\mathbf{a}=\frac{C}{2N_x} \qquad [17.11]$$

Equation 17.9 is the basis of the shape effect and leads to the idea of the relrod, which you recall is the name we give to a reciprocal lattice rod.

17.1.B. The Integration Approach

If we take equation 13.2, which is the amplitude diffracted by a single unit cell, and sum this over all the cells in the specimen, the amplitude of the diffracted beam can be written as

$$\phi_{\mathbf{g}}=\frac{e^{2\pi i\mathbf{k}\cdot\mathbf{r}}}{r}\sum_n F_n e^{\left(-2\pi i\,\mathbf{K}\cdot\mathbf{r}_n\right)} \qquad [17.12]$$

Since we have defined $\mathbf{K}$ to be $\mathbf{g}+\mathbf{s}$, we can rewrite this equation as

$$\phi_{\mathbf{g}}=\frac{e^{2\pi i\mathbf{k}\cdot\mathbf{r}}}{r}\sum_n F_{\mathbf{g}} e^{\left(-2\pi i\,(\mathbf{g}+\mathbf{s}_{\mathbf{g}})\cdot\mathbf{r}_n\right)} \qquad [17.13]$$

Now we know that $\mathbf{g}\cdot\mathbf{r}_n$ is an integer by the definition of $\mathbf{g}$ and $\mathbf{r}_n$ and we will refer to $\mathbf{s}_{\mathbf{g}}$ as $\mathbf{s}$. Hence we can write equation 17.13 as

$$\phi_{\mathbf{g}}=\frac{e^{2\pi i\mathbf{k}\cdot\mathbf{r}}}{r}\sum_n F_{\mathbf{g}} e^{\left(-2\pi i\,\mathbf{s}\cdot\mathbf{r}_n\right)} \qquad [17.14]$$

where $\mathbf{s}$ is the deviation parameter for reflection $\mathbf{g}$. If we make the approximation that the crystal contains many unit cells, we can replace this sum by an integral to give

$$\phi_{\mathbf{g}}=\frac{e^{2\pi i\mathbf{k}\cdot\mathbf{r}}}{r\,V_c}F_{\mathbf{g}}\int_{\text{crystal}} e^{\left(-2\pi i\,\mathbf{s}\cdot\mathbf{r}_n\right)}dv \qquad [17.15]$$

This is where the present treatment differs from the first. If we now express $\mathbf{s}$ and $\mathbf{r}_n$ as the vectors

$$\mathbf{s}=u\mathbf{a}^*+v\mathbf{b}^*+w\mathbf{c}^* \qquad [17.16]$$

and

$$\mathbf{r}_n=h\mathbf{a}+k\mathbf{b}+\ell\mathbf{c} \qquad [17.17]$$

then we can write

$$\phi_{\mathbf{g}}=\frac{e^{2\pi i\mathbf{k}\cdot\mathbf{r}}}{r\,V_c}F_{\mathbf{g}}\int_0^C\int_0^B\int_0^A e^{\left(-2\pi i\,(ux+vy+wz)\right)}dx\,dy\,dz \qquad [17.18]$$

where $A=N_x a$, etc. This integral is straightforward

$$\begin{aligned}\int_0^A e^{-2\pi iux}&=\frac{e^{-2\pi iuA}-1}{-2\pi iu}=\left(\frac{e^{-\pi iuA}}{\pi u}\right)\left(\frac{e^{\pi iuA}-e^{-\pi iuA}}{2i}\right)\\&=\frac{e^{-\pi iuA}}{\pi u}\sin(\pi uA)\end{aligned} \qquad [17.19]$$

$$\phi_{\mathbf{g}}=\frac{e^{2\pi i\mathbf{k}\cdot\mathbf{r}}}{r\,V_c}F_{\mathbf{g}}\frac{(\sin\pi Au)}{(\pi u)}\frac{(\sin\pi Bv)}{(\pi v)}\frac{(\sin\pi Cw)}{(\pi w)}e^{iD} \qquad [17.20]$$

(D is an unimportant phase factor.) The intensity is then as given by equation 17.9, but we have explicitly kept the r^{-2} and V_c^{-2} dependence for the intensities.

You should recognize the form of equations 17.9 and 17.20. These equations have the same form as that given in equation 2.12 for the diffraction from a diffraction grating. The corresponding diffraction grating has N_x lines which are spaced a distance a apart. The physical

similarity is that the grating, just like our crystal, has a finite size.

17.2. THE THIN-FOIL EFFECT

Equation 17.9 is very important for TEM. It tells us why the relrods we introduced in Chapter 12 have a finite length if we measure them to the first minimum. It also tells us that the diffracted intensity does depend on the value of **s**; it is not a constant for any position along the rod.

We can better appreciate this variation along the rod if we plot the intensity and draw the Ewald sphere, as shown in Figure 17.2. We only draw the intensity plot for one direction at a time. This diagram shows the Ewald sphere cutting the relrod on one side while showing the intensity along the relrod on the right-hand plot.

Just remember that when we said intensity in the last sentence, we meant:

> The intensity which the diffracted beam will have if **s** takes a particular value; i.e., if the Ewald sphere cuts the relrod at that point.

In other words, Figure 17.2 is an extension of Ewald's "pictorial representation" of diffraction. We can now draw the reciprocal lattice as shown for a simple-cubic crystal in Figure 17.3, such that every point is replaced by a relrod and every relrod is described by equation 17.9. If the surface of the crystal is exactly parallel to the (112) plane, but we orient the specimen slightly off the [001] pole, then the Ewald sphere cuts the relrod at different positions relative to the square array which is the projection of the spots at zero tilt (Figure 17.3B). The DP will appear as shown in Fig-

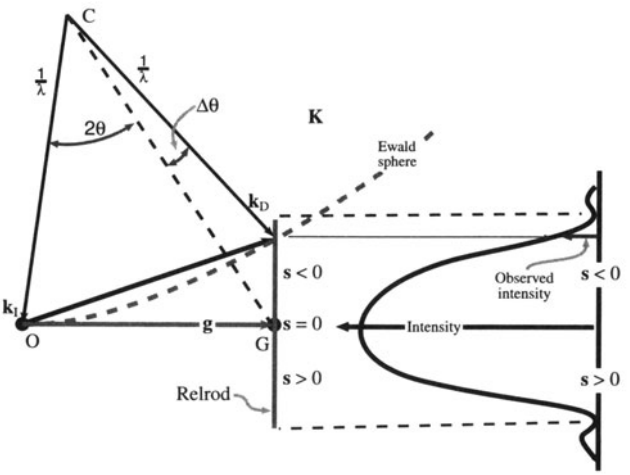

Figure 17.2. The relrod at $\mathbf{g}_{hk\ell}$ when the beam is Δθ away from the exact Bragg condition. The Ewald sphere intercepts the relrod at a negative value of **s** which defines the vector **K** = **g** + **s**. The intensity of the diffracted beam as a function of where the Ewald sphere cuts the relrod is shown on the right of the diagram. In this case the intensity has fallen almost to zero.

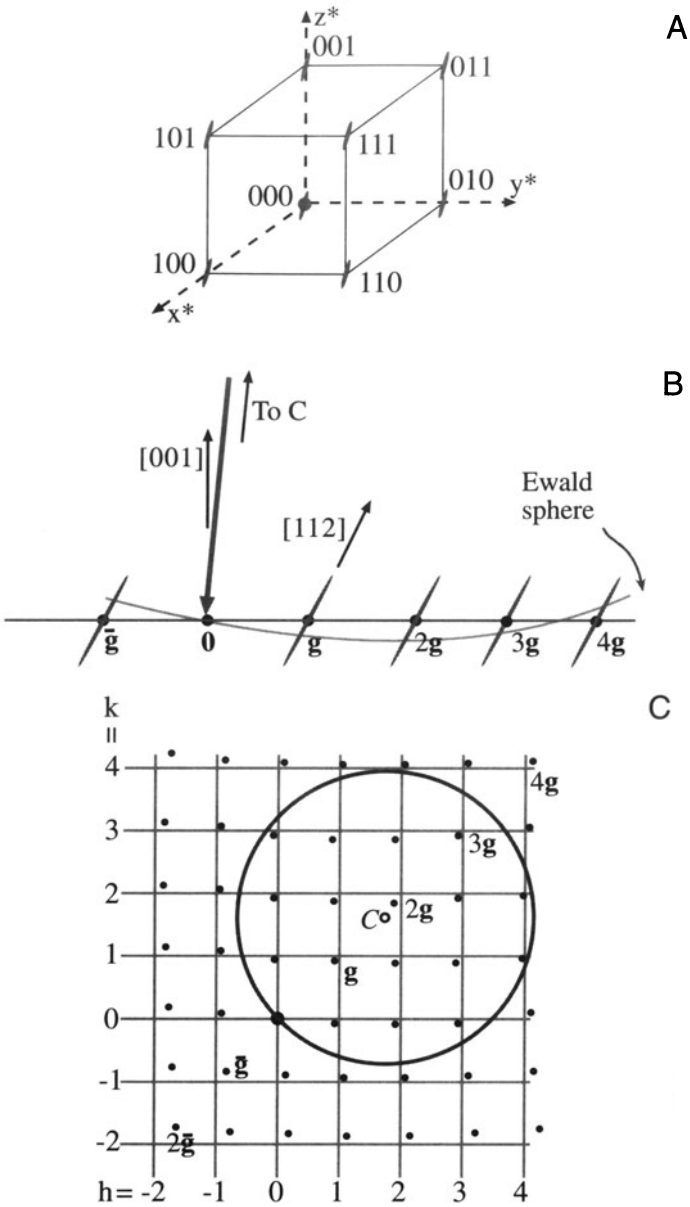

Figure 17.3. (A) For a thin specimen, every point is replaced by a relrod. (B) The Ewald sphere cutting the relrods in (A) when the crystal is tilted slightly off the 001 axis. (C) The effect of the tilt in (B) on the DP. Notice that all of the spots in the DP are displaced relative to their positions on the square grid (the projection of the spots at zero tilt), but that the magnitude of the displacement varies depending on the sign and size of **s**. Of course, spots on the Ewald sphere must still be the "correct" distance from 000.

ure 17.3C. In Figure 17.3C, C is the projected position of the center of the Ewald sphere. As an exercise, consider whether the pattern would differ if the surface were cut slightly off (001) but oriented at the [001] pole. Then repeat the first exercise but instead of tilting the specimen, tilt the electron beam through the same small angle.

Remember that we deduced equation 17.9 by simply adding the amplitudes from all the unit cells, taking the position of the cells into account.

> We calculated a "structure factor" for the whole volume which contributes to ϕ_g: we call this calculated factor the shape factor.

We should then use this shape factor rather than the structure factor (since F is included in equation 17.9) in our dynamical calculations of ϕ_g. The problem is, of course, that the shape factor can be different for every specimen we examine.

We have just deduced a method for picturing how the shape of a perfect parallelepiped (of sides $N_x a$, $N_y b$, and $N_z c$) affects the DP. Now for the next step, we will use this concept of the shape factor to examine how the DPs will be affected by more complex shapes, such as the wedge shape of many real TEM specimens or the perfect parallelepiped of the stacking fault. Then we will consider defects which themselves do not have sharp boundaries; the dislocation is a perfect example of such an imperfection.

17.3. DIFFRACTION FROM WEDGE-SHAPED SPECIMENS

Most TEM specimens do not have parallel surfaces but are wedge-shaped. In drawing the relrods for such a wedge-shaped specimen, we extend the results of Section 17.2 by saying that the relrod will always be normal to the surface. So, for a wedge-shaped specimen (Figure 17.4A) we must have two relrods, as shown in Figure 17.4B. What we see in the DP is determined by how the Ewald sphere cuts these two relrods. As shown in Figures 17.4C, D, we will see two spots which lie along a line which is normal to the edge of the wedge. Notice that all the pairs of spots are aligned in the same direction as we expected and that their separation is larger for larger values of **s**. This simple relrod model predicts that we would see only one spot if $\mathbf{s} = 0$. In fact, we should see two or more spots because the relrod model fails when we are in a strong dynamical-diffraction condition. We will return to this point in the next section and again in Chapter 24.

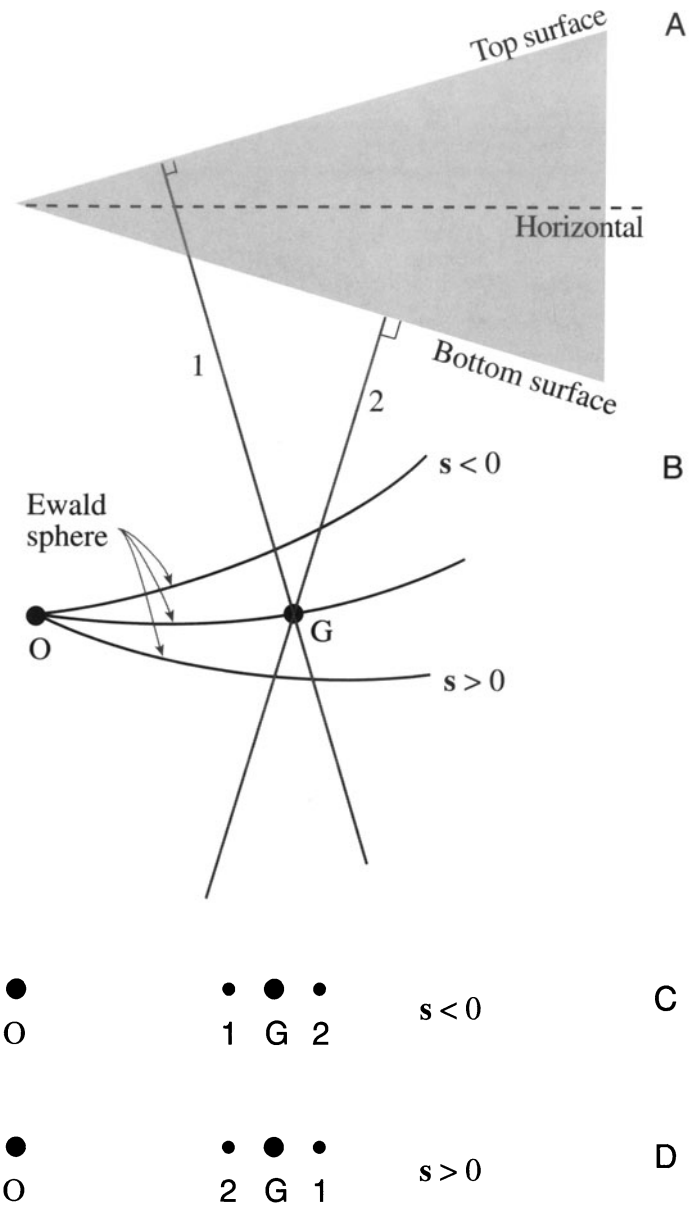

Figure 17.4. (A) Diffraction from a wedged crystal. (B) Notice that when $\mathbf{s} < 0$, relrod 1 is on the left of relrod 2 but the order reverses when **s** becomes >0. The effect of this pair of relrods is to create a doublet shown in (C) and (D). The middle spot is the matrix relrod.

17.4. DIFFRACTION FROM PLANAR DEFECTS

The shape factor concept can be readily applied to understand diffraction from a flat platelet or planar fault, such as the geometry shown in Figure 17.5. The idea is that the platelet is itself a thin parallelepiped which is inclined to

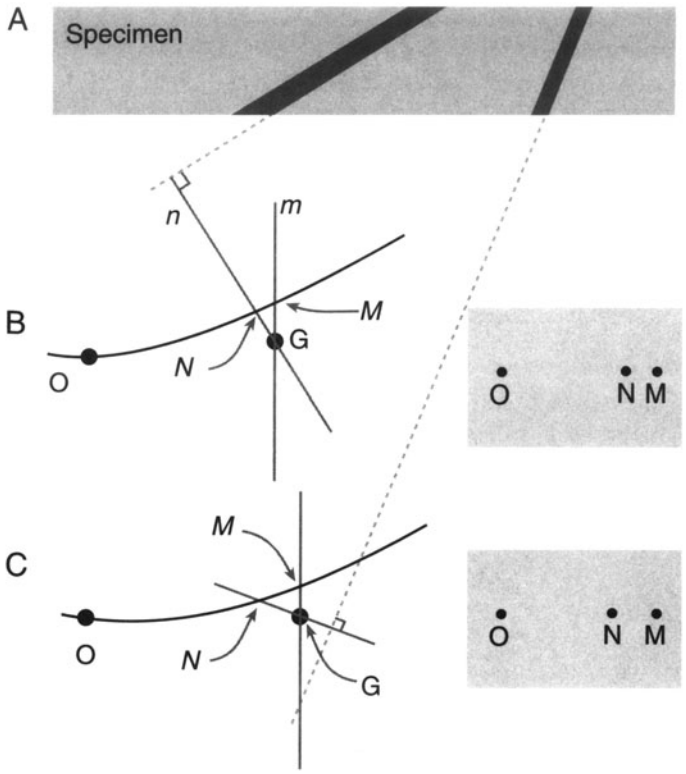

Figure 17.5 The effect of a thin inclined plate in a thin specimen. (A) Two plates are shown to illustrate the effect of changing the inclination of the plate relative to the foil surface. When $\mathbf{s} \neq 0$ we see two spots in the DP because there are two relrods for the two different planar-defect inclinations in (B) and (C).

the specimen parallelepiped (Figure 17.5A). The result is that we have two relrods, one normal to the specimen surface and a much longer one normal to the thin platelet (Figure 17.5B). When we cut these relrods with the Ewald sphere we produce two spots in the DP and, as for the wedge specimen, the separation of the spots increases with increasing **s**. The line MN lies normal to the trace of the platelet. There are, however, some differences in this case. Although the *m* and *n* relrods are very different in length and actual intensity, the diffracting volume is much greater for the specimen than for the platelet. Thus, we can usually distinguish reflections M and N.

Providing we know the orientation of the specimen relative to the DP, we can tell whether the inclination angle is less than or greater than 90°; i.e., we can determine the inclination of the planar defect without moving the specimen or using any theory of image contrast (see Chapter 24). As in Section 17.3, we actually see two spots when **s** = 0, and we'll return to this topic in Section 17.7.

A stacking fault in an fcc crystal can be thought of as a very thin platelet of hcp material, as shown in Figure 17.6; so it really is a platelet with perfect lattice matching parallel to its surface.

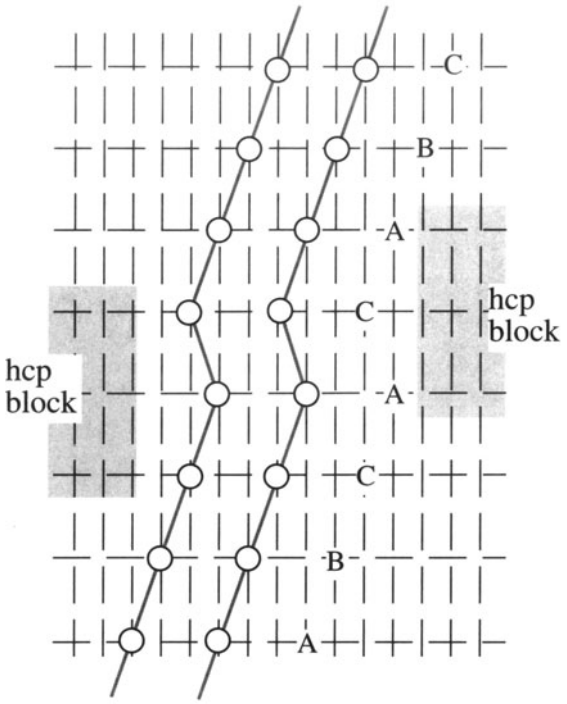

Figure 17.6 Schematic of the stacking sequence of close packed planes A, B, C, in an fcc crystal showing that the SF is similar to a thin layer of hcp material, stacking ACA.

We can understand diffraction effects from other planar interfaces by considering two cases:

- If the grains on either side of the interface contain a common reflection, then the diffraction effects can be modeled by the thin platelet.
- In the case where a reflection is not common to the two grains, then for that reflection the diffracting crystal behaves like a wedge specimen with one surface parallel to the planar defect. We can ignore the crystal that is not diffracting.

The two DPs in Figure 17.7 show that you really do see pairs of spots for these two types of boundary. As before, the two spots lie normal to the boundary traces, i.e., the intersection of the boundary with the surface of the specimen.

There are two reasons for emphasizing the extra spots which are present because of the interface:

- You should always check that any extra spots you see cannot be explained in this way.

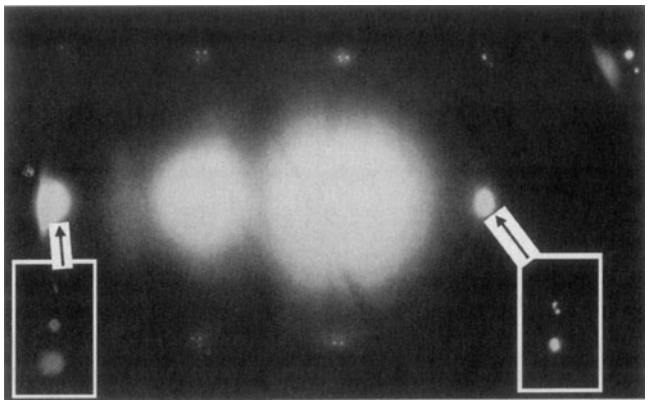

Figure 17.7. Pairs of spots in a DP from a grain boundary.

- You must be careful when determining spot spacing (as when estimating lattice parameters). You must set **s** to zero for this purpose, and that can usually only be done for a few reflections at any time (one reflection always being **0**, of course).

Twin boundaries are often found to consist of flat segments in particular orientations. The first-order twin boundary in fcc crystals tends to facet parallel to the common {111} plane, as shown schematically in Figure 17.8A. This means that if we orient the specimen so that this common plane is nearly parallel to the beam, we will excite the common {111} reflection. Now, our platelet is parallel to the beam so that its relrod is normal to the beam. If the specimen is also thin, we can arrange that the Ewald sphere cuts along the length of the relrod. Now, as you can see in Figure 17.8B, there is a "streak" in the DP rather than a spot. The streak actually extends in the [111] direction because, as you can appreciate from Figure 17.8A, the twin is a *very* thin platelet.

If we regard the surface as a planar defect, we can also observe extra spots in the DP due to a reconstruction of the surface. One factor to be cautious about is that the apparent reconstruction might be influenced by contamination since the TEM is not generally a UHV system.

A

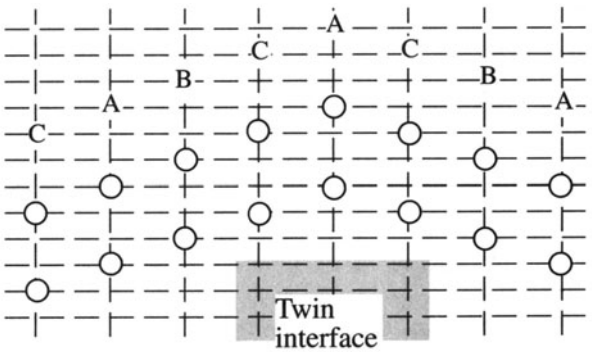

B

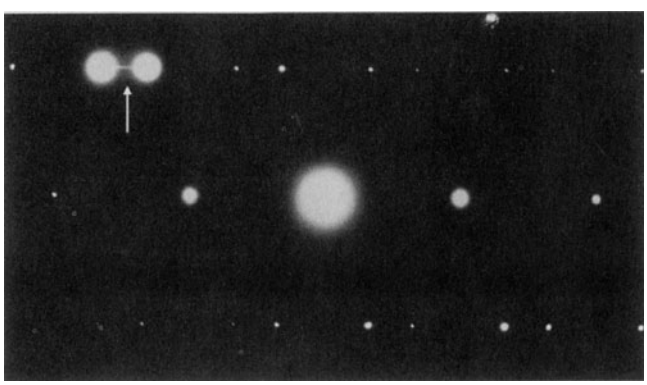

Figure 17.8. (A) Schematic of twin and (B) DP with a streak (arrowed) normal to the twin plane. Note that **s** = 0 for the two bright diffracted spots.

17.5. DIFFRACTION FROM PARTICLES

Particles come in all shapes and sizes, so we will not try to be exhaustive. Actually, the principles involved in determining the shape factor in reciprocal space are simply "small becomes large" and vice versa. The shape factors are shown schematically for several particles in Figure 17.9. You should be aware that you will probably never see the subsidiary maxima shown in these diagrams.

One example, which is common, is the platelets shown in Figure 17.10; these can occur as GP zones or other thin disk-shaped precipitates. When the platelets are oriented parallel to the beam, we see streaks in the DP, just as we saw them in Figure 17.8B. The difference in this figure is that the platelets can lie on all the crystallographically equivalent planes in the crystal. For these GP zones they lie on {001} planes, so the streaks run in <001> directions for the cubic crystal connecting, for example, 000 and 200. You should notice that these spots would still be connected if the crystal were not cubic. You'll also see that there is a sharp point at the 100 position, even though 100 is not an allowed reflection for bcc crystals. The reason we see this spot is that we are cutting the relrod which runs parallel to the electron beam in the [001] direction.

The smallest "particle" can be thought of as a vacancy, a substitutional atom, or an interstitial atom. We will not expect to see any clear effect of a single point defect but, as we saw in Section 16.7, these point defects can order to give a clear superlattice, and therefore extra spots.

As you might expect then, if we have many point defects but not enough to give long-range order, we might expect short-range ordering. Perhaps the clearest example of this phenomenon again occurs in the metal carbides. The effect is shown in Figure 17.11. The short-range ordering gives rise to diffuse scattering in the DP which at first appears quite

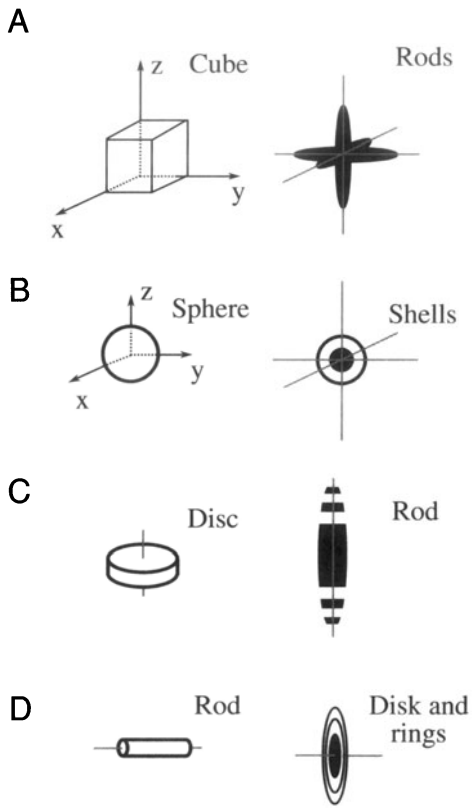

Figure 17.9. Examples of how spots in reciprocal space have different shapes, depending on the shape of the particles which are diffracting.

random, sometimes as circles around the spots and appearing at other times as circles between spots or not circles at all! By combining many different patterns, Sauvage and Parthé (1972) proposed that the diffuse scattering could be mapped out as shown in Figure 17.11D. This figure strongly resembles a Fermi surface diagram, which you may have encountered in solid-state physics. We will discuss some aspects of imaging using diffusely scattered electrons in Section 31.4, but the important points to recognize are:

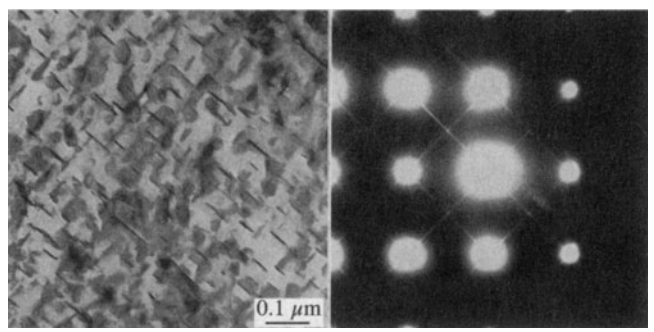

Figure 17.10. Very thin plate-like precipitates (A) cause long streaks in the DP (B). In this example, the precipitates are GP zones in an Fe-2.9 at % Mo alloy.

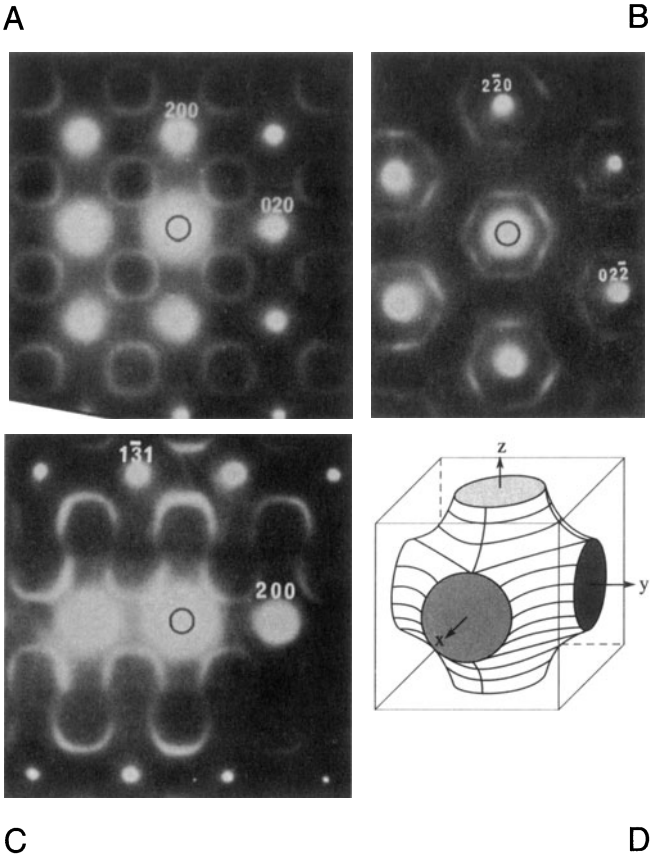

Figure 17.11. Short-range ordering can cause diffuse scattering in the DP (A–C). The DPs in this example were obtained from a vanadium carbide. In this case, the 3D map of diffuse intensity has a shape which strongly resembles a Fermi surface, shown in (D).

- Point defects can cause diffraction effects, especially if they interact with one another.
- Diffuse scattering can still be interpreted by the Ewald sphere construction.

If you are intrigued by this topic, you will find the literature on discommensurate structures in intercalated material a complementary challenge (Wilson *et al.* 1975). A library search on "discommensurate" and "intercalated" should quickly net any more recent papers.

17.6. DIFFRACTION FROM DISLOCATIONS, INDIVIDUALLY AND COLLECTIVELY

In Chapter 25 we will discuss images of dislocations. A dislocation is a line defect which is characterized by its line direction and its Burgers vector. The crystal around the defect is distorted or strained.

For a single dislocation, this strain is not expected to cause new spots in the DP, but we do expect diffuse scattering since the dislocation is a line defect. If a region from 2 Å to 10 Å around the core is greatly distorted (we'll see the effect of this strain in Chapter 25), then the diffuse scattering will extend from 0.1 $Å^{-1}$ to perhaps 0.5 $Å^{-1}$ from the reciprocal lattice points, giving a diffuse disk (the reciprocal shape of a long needle). Some planes are essentially unaffected by the dislocations, so we might expect the diffuse scattering to vary in magnitude for the different reciprocal lattice points.

With this simple discussion and without ever seeing this diffuse scattering, we can draw an important conclusion: if we want to learn about the structure of a dislocation core, we must include the diffuse scattering in the image formation process. We must include that intensity in the objective aperture and the corresponding image calculations.

This diffuse intensity is *not* located at the reciprocal lattice point.

Because the distorted volume associated with a single dislocation is so small, we do not expect to see this intensity in the DP unless we have many dislocations. We can demonstrate that this intensity is present by diffracting from an ordered array of dislocations, as shown in Figure 17.12. The specimen used to form this image was rather special. Dislocations are present in region A, but not in region B. The array actually forms a structured grain boundary in A, but a layer of glass is present in B. The insets show the same part of the SAD patterns from the two regions. In B, you can see three spots. The top two are from one grain, the bottom one is from the other grain. The reason for the pair of spots is that **s** is large for that grain, but almost zero for the other. This is an example of the application of Section 17.3.

In A, you see the same three spots (because the grains are still present) but now there are two extra spots. The reason you see two extra spots is that we have two arrays of dislocations. You are seeing the scattering from the dislocations because they have formed an array with long-range ordering, just like the vacancies in V_8C_7 in Chapter 16.

If you look at the DP when the array of dislocations lies parallel to the beam, you may be able to see a set of streaks as shown in Figure 17.13. The separation of the

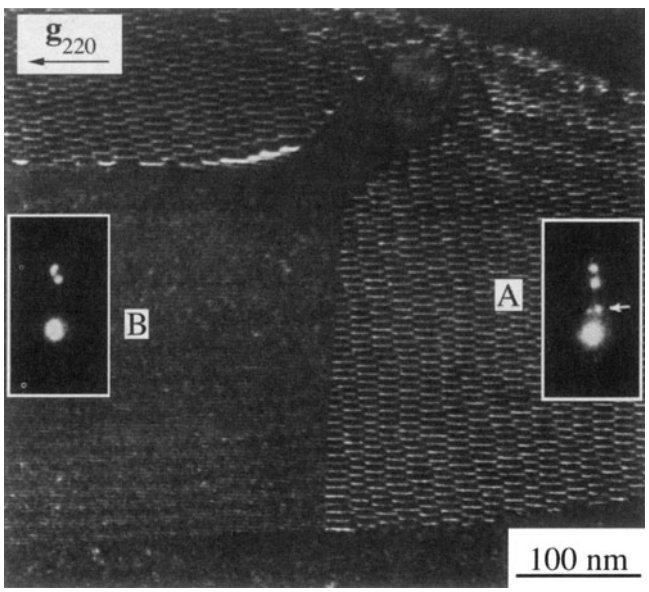

Figure 17.12. Diffraction from an ordered array of dislocations. Dislocations are present in region A, but not in B. The insets show a small part of the DP from the two regions. The extra spots arrowed in A are caused by the visible array of dislocations; these spots are a doublet because there is also a second, nearly orthogonal, set of dislocations present which acts as a separate grating. The other pair is due to the wedge shape and so is common to both DPs.

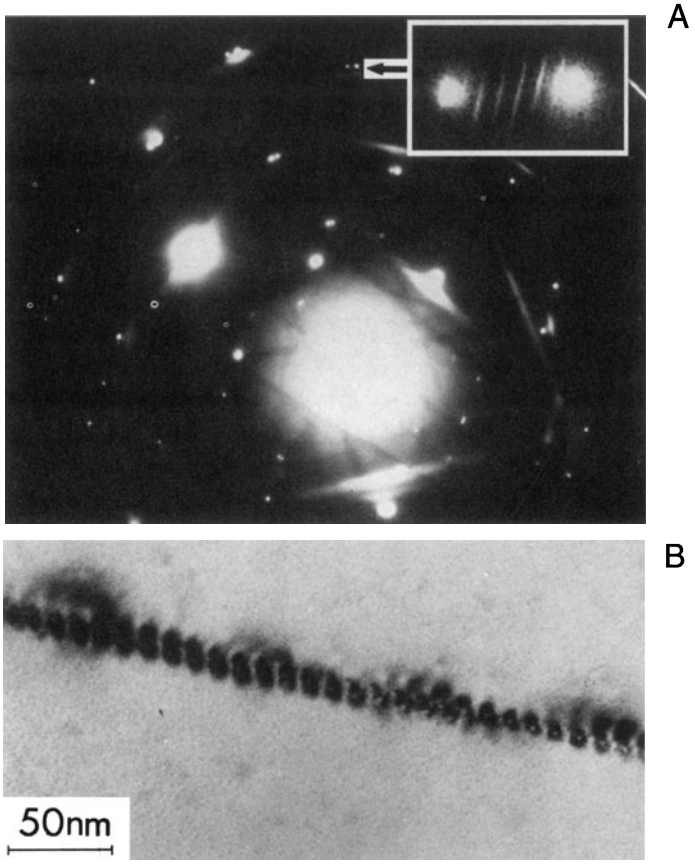

Figure 17.13. (A) The set of streaks from an array of dislocations in Al_2O_3 lying parallel to the electron beam. The distance between the streaks is inversely related to the spacing of the dislocations shown in the image (B).

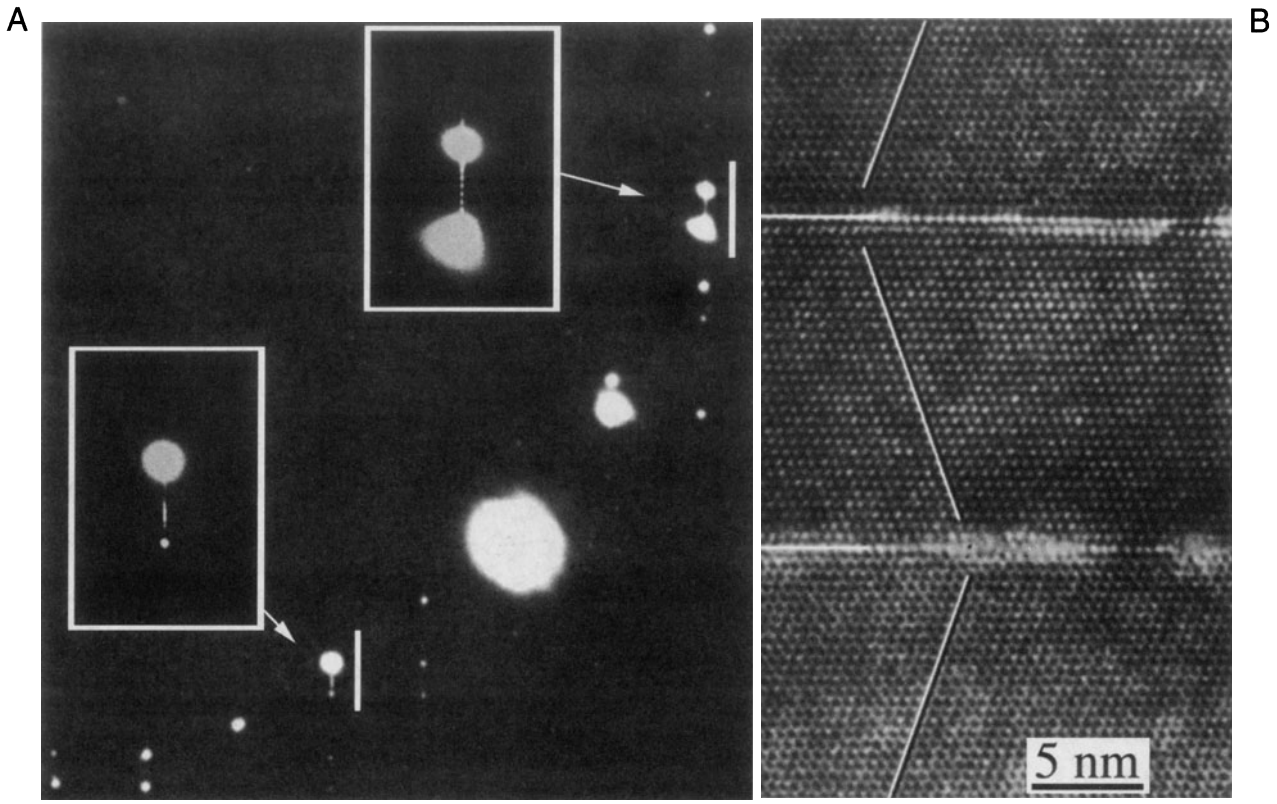

Figure 17.14. Extra spots can be formed in the DP (A) when only two defects are scattering in phase. The separation of the extra spots is related to the inverse of the separation of the two twin boundaries seen in the image (B).

streaks is the inverse of the actual separation of the dislocations. You see streaks because you have relrods in reciprocal space and we are cutting along these rods with the Ewald sphere. The length of the relrods gives you a measure of how far the strain field of the dislocations extends out into the two grains. In other words, we are seeing a thickness of the strain-field regions. The object of this discussion is not to examine grain boundaries, but to show that the strain field from an array of dislocations causes scattering in the DP and thus to infer that one dislocation will also cause scattering, but it will just be much more diffuse.

Before moving on, consider the diffraction spots in Figure 17.12 again. Why are the pairs of dislocation spots (arrowed) located where they are? Put another way: which of the two spots in region B corresponds to the N relrod and which corresponds to the M relrod? (See Figure 17.5 for the definition of M and N.)

The general rule is:

> If there is a structural periodicity in real space, then there will be an array of points or relrods in reciprocal space and an array of spots or streaks in the DP.

We then ask a simple question: how many objects are required in order to produce a detectable effect in the DP? The answer is two! This point is illustrated in Figure 17.14, which shows a DP and an image of two twin boundaries which are ~15 nm apart. The spacing of the new spots between the twin spots in the DP (expanded in the insets) is 0.067 nm^{-1}, as expected. Now, why can this occur? The analogy is Young's slits experiment in visible-light optics (Carter 1984). The illustration also reminds us of a special feature of the TEM, namely, that even without an FEG, the electron beam is remarkably coherent.

17.7. DIFFRACTION AND THE DISPERSION SURFACE

Several times in this chapter, we have said "actually, you will see two spots when $\mathbf{s} = 0$," even though the relrod model says that you will only see one. The origin of two spots (there may be more for more complicated defects) is due to the dynamical nature of the scattering process. The theory has been derived by Amelinckx and his co-workers in a series of papers. For a full introduction, we recom-

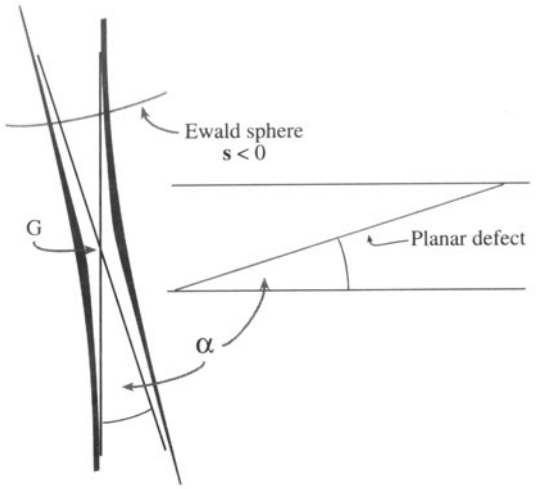

Figure 17.15. The relrods from two planes inclined at angle α are actually asymptotic to two straight lines, so that they don't cross at G; when **s** = 0, the distance between these two curves is ξ_g^{-1}.

mend the review by Gevers (1971). Unfortunately, this group used a different notation, but they did summarize their results graphically. We will also return to this topic when we discuss images in Chapter 24. As an example, the relrod diagram given for the stacking fault in Figure 17.5 should be drawn so that the relrods are asymptotic to two straight lines, as shown in Figure 17.15. When the Ewald sphere cuts these curves at **s** = 0, we see that there are two spots which move apart as we increase **s** (either positive or, as shown here, negative) until they are at the points defined by the straight lines. So, will there be a vector that exactly corresponds to **g**? The answer, of course, is yes, because of the adjacent perfect crystal, so we must have three spots, but these are very difficult to see because **s** must be very close to zero. Without going into any theory, we can guess the origin of these curves: they look remarkably like the curves of the dispersion surface which also had asymptotes (see Figure 15.3). These curves are indeed directly related.

When you increase **s**, you move out of the dynamical regime and into the kinematical one, where the simple relrod model applies (see Chapter 26). At **s** = 0, the distance between the curves is inversely proportional to ξ_g, the extinction distance for reflection **g**.

You can understand why this is so in the following pictorial way. What you see in the image will be determined by the DP. What you see in the DP is determined by which relrods, or surfaces, the Ewald sphere intersects. All the information about extinction distances and coupling of diffracted beams is fundamentally contained in the dispersion surface (ξ_g is just Δk^{-1} at **s** = 0). Both the dispersion-surface and the reciprocal-lattice/Ewald-sphere models are just pictorial representations of the same diffraction process. So, all the information in the dispersion-surface model should also be present in the reciprocal-lattice/Ewald-sphere model.

The relrods are the asymptotes to these two hyperbolas. Alternatively, we could say that the relrods and the asymptotes are a result of the kinematical diffraction approximation. There is a one-to-one correlation between what happens at the dispersion surface in the vicinity of the BZB and what happens when the Ewald sphere cuts the relrods in the vicinity of the reciprocal lattice point, G. Imagine rotating the dispersion-surface diagram through 90°. These ideas have been extensively studied by van Landuyt, de Ridder, Gevers, Amelinckx *et al.*, as summarized in the general references at the end of this chapter. What Amelinckx's group has done is to give us the rules on how to transfer this information from the dispersion surface to the reciprocal lattice and hence to the DP. In Section 24.9 we'll relate this concept to images. If you thought dispersion surfaces were difficult, make **s** large and stick to relrods!

CHAPTER SUMMARY

In this chapter, we have begun to examine the unique features of diffraction in the TEM. These features arise because we are always diffracting from small volumes. The sizes of both our specimen and the special features present in our specimen are always small, so that you must take into account the shape effect. Of course, the same considerations will also apply to other forms of diffraction, it's just that only TEM can examine the diffraction information from the vicinity of crystal defects. In other words, the shape effect is not a limitation due to the fact that we are using high-energy electrons. By understanding the concept of the shape effect you can actually learn more about defects in crystals; conversely, you can make some major errors if you do not understand the shape effect. Two points to remember are:

- When a platelet is parallel to the beam, its relrod is normal to the beam. If the specimen is also thin, you can arrange that the Ewald sphere cuts along the length of the relrod. Now you'll see a "streak" in the DP rather than a spot.
- Beam splitting at **s** = 0 and the dispersion surface both arise because of dynamical scattering.

REFERENCES

General References

The relation between diffraction and images from planar defects has been the subject of a long series of papers. The following will give you a start to your study.

de Ridder, R., Van Landuyt, J., Gevers, R., and Amelinckx, S. (1968) *Phys. stat. sol.* **30**, 797; (1970) *ibid.* **38**, 747; (1970) *ibid.* **40**, 271; (1970) *ibid.* **41**, 519; (1970) *ibid.* **42**, 645.

Gevers, R., Van Landuyt, J., and Amelinckx, S. (1966) *Phys. stat. sol.* **18**, 343; (1967) *ibid.* **21**, 393; (1967) *ibid.* **23**, 549; (1968) *ibid.* **26**, 577.

Van Landuyt, J. (1964) *Phys. stat. sol.* **6**, 957.

Van Landuyt, J., Gevers, R., and Amelinckx, S. (1966) *Phys. stat. sol.* **13**, 467; (1966) *ibid.* **18**, 167.

Specific References

Carter, C.B. (1984) *Phil. Mag.* **A50**, 133.

Gevers, R. (1971) in *Electron Microscopy in Materials Science* (Ed. U. Valdrè), p. 302, Academic Press, New York.

Sauvage, M. and Parthé, E. (1972), *Acta Cryst.* **A28**, 607.

Wilson, J.A., Di Salvo, F.J., and Mahajan, S. (1975) *Adv. Phys.* **24**, 117.